Geoscience Frontiers 12 (2021) 101114

HOSTED BY

Contents lists available at ScienceDirect

Geoscience Frontiers

journal homepage: www.elsevier.com/locate/gsf

Research Paper

Oceanic lithosphere heterogeneity in the eastern Paleo-Tethys revealed by PGE and Re–Os isotopes of mantle peridotites in the Jinshajiang ophiolite

Yan-Jun Wang [a,b], Wen-Jun Hu [b,c,*], Hong Zhong [b,d], Wei-Guang Zhu [b], Zhong-Jie Bai [b]

[a] State Key Laboratory of Nuclear Resources and Environment, East China University of Technology, Nanchang 330013, China
[b] State Key Laboratory of Ore Deposit Geochemistry, Institute of Geochemistry, Chinese Academy of Sciences, Guiyang 550081, China
[c] Department of Earth Sciences, The University of Hong Kong, Hong Kong, China
[d] College of Earth and Planetary Sciences, University of Chinese Academy of Sciences, Beijing 100049, China

ARTICLE INFO

Article history:
Received 29 February 2021
Received in revised form 11 August 2020
Accepted 20 November 2020
Available online 17 December 2020

Handling Editor: Kristoffer Szilas

Keywords:
Jinshajiang ophiolite
Paleo-Tethys
Mantle peridotites
Melt-rock reaction

ABSTRACT

Platinum group elements (PGE) and Re–Os isotopes of mantle peridotites in the Jinshajiang ophiolite (SW China) were investigated in this study, in order to constrain the evolution of the lithospheric mantle beneath the Jinshajiang-Ailaoshan Ocean, which was a branch of the eastern Paleo-Tethys. The Jinshajiang peridotites have whole-rock compositions (e.g., MgO = 32.7–38.1 wt.%; Al_2O_3 = 0.67–1.30 wt.%) and spinels with moderate Cr# values (0.4–0.6) similar to those of abyssal peridotites, which indicate moderate degrees of partial melting (15%–20%). These peridotites exhibit U-shaped chondrite-normalized REE patterns that could be caused by hydrothermal alteration or melt-rock interaction after mantle melting. In addition, Pd concentrations and $(Pd/Ir)_N$ ratios of the Jinshajiang peridotites increases with decreasing Al_2O_3 concentrations. These negative correlations cannot be explained by simple partial melting but record a melt-rock reaction event after mantle melting. This study therefore demonstrates the efficiency of PGE in detecting the melt-rock reaction process relative to whole-rock major and trace elements. The suprachondritic $^{187}Os/^{188}Os$ ratios (0.1272–0.1374) further indicate that the later percolating melt derived from a mantle domain with distinct ^{187}Os-enriched isotopic compositions. In comparison with peridotites in the Ailaoshan ophiolite belt, which were not significantly affected by melt percolation, this study further highlights that the lithospheric mantle compositions beneath different segments of the same ocean basin are highly variable and might be controlled by distinct mantle processes in response to different rifting mechanisms.

1. Introduction

Ophiolites are fragments of ancient oceanic lithosphere which were formed in a variety of tectonic settings and then incorporated into continental margins during convergent processes of plates (Dilek and Furnes, 2011). Therefore, ophiolites are crucial for reconstruction of plate tectonics, because they mark sutures between boundaries of different amalgamated plates or accreted terranes and are the only remnants of ancient oceanic lithosphere (Dilek and Furnes, 2011, 2014; Pearce, 2014). An intact ophiolite sequence comprises a lower lithospheric mantle section and an upper igneous crustal section with minor abyssal sediments (Dilek and Furnes, 2011). The crustal section is widely applied to determine the formation age of the ophiolite and rebuild tectonic environment and evolution of oceanic lithosphere (Pearce, 2014). For instance, the development of sheeted dikes neighboring the tabular intrusions of magma within ophiolite belt indicates the seafloor spreading event, whereas crustal sequence with geochemistry akin to arc magmatism is indicative of the closure of oceanic basins (Dilek and Furnes, 2011). However, chemical compositions of igneous crusts are often modified by processes after magma generation, e.g., crustal assimilation, which possibly misleads the final interpretation. In comparison, mantle peridotites in ophiolites are more direct to learn the evolution of oceanic lithosphere. Compared with mantle xenoliths and abyssal peridotite, mantle peridotites in ophiolites allow more systematic sampling and provide better opportunities to observe the structural relations between the mantle section and the crustal section (Bodinier and Godard, 2003). Mantle peridotites in ophiolites can record different stages of oceanic lithosphere (e.g., Xu et al., 2020), from formation, subsequent modification to final accretion (e.g., Xiong et al., 2016, 2017; Liu et al., 2019a; Zhang et al., 2016, 2019). Investigations on ophiolites and modern oceanic lithosphere reveal that the oceanic lithosphere is chemically and isotopically heterogeneous in

* Corresponding author at: State Key Laboratory of Ore Deposit Geochemistry, Institute of Geochemistry, Chinese Academy of Sciences, Guiyang 550081, China.
E-mail address: huwenjun170@163.com (W.-J. Hu).

https://doi.org/10.1016/j.gsf.2020.11.011

different scales (e.g., O'Driscoll et al., 2012; Rampone and Hofmann, 2012), which could be attributed to different mantle processes, including variable melting, melt-rock reaction, refertilization and lithospheric recycle (Parkinson et al., 1998; Harvey et al., 2006; Liu et al., 2008; O'Reilly et al., 2009; Rudnick and Walker, 2009; Schulte et al., 2009; Lorand et al., 2013; Xiong et al., 2016, 2017).

The Sanjiang (three rivers: Nujiang, Lancangjiang and Jinshajiang) area in SW China records the final consumption of the eastern Paleo-Tethys Ocean (Mo et al., 1998; Zhong, 1998; Metcalfe, 2006, 2011, 2013; Deng et al., 2014). Several ophiolitic belts occur along the N-S tectonic lines (Fig. 1). The Lancangjiang ophiolitic belt is considered as the suture of the Paleo-Tethys Main Ocean, while the Jinshajiang-Ailaoshan ophiolitic belt is defined as the remnant of a branch ocean (i.e., the Jinshajiang-Ailaoshan Ocean) (Jian et al., 2008, 2009b; Zi et al., 2012c). Extensive efforts have been made concerning about the geochronology and tectonic reconstruction of the eastern Paleo-Tethys Ocean based on crustal igneous rocks within these ophiolites (Wang et al., 2000a, 2012, 2018; Jian et al., 2008, 2009a, b;; Xiao et al., 2008; Zi et al., 2012a, b, c; Hu et al., 2015, 2019). However, the nature of mantle peridotites therein was poorly studied. A recent study by Hu et al.

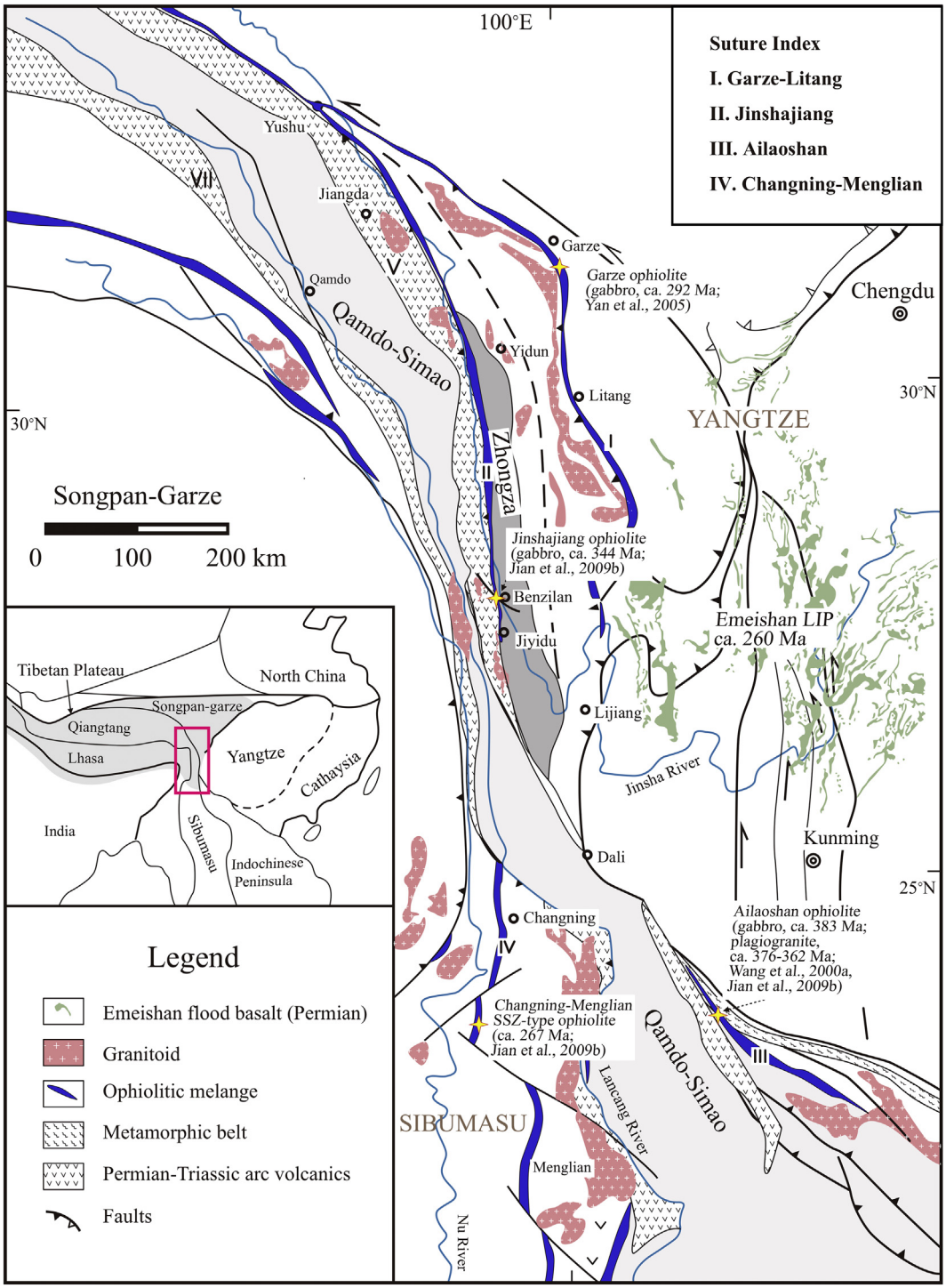

Fig. 1. Geological map of Paleo-Tethys suture zones (ophiolitic belts) and tectonic units in the Sanjiang area, southwest China (after Zi et al., 2012b).

(2020) reported systematic platinum group elements (PGE) and Re–Os isotopes of mantle peridotites in the Ailaoshan ophiolite, and proposed that the mantle heterogeneity beneath the Ailaoshan segment may be caused by incorporation of subcontinental lithospheric mantle into the upwelling asthenosphere during the rifting of the segment (O'Reilly et al., 2009; Liu et al., 2015; Scott et al., 2019). We here present a set of data including mineral compositions and whole-rock PGE and —Re–Os isotopes for the Jinshajiang peridotites, which provide information of lithospheric mantle beneath the Jinshajiang segment and allow further regional comparison with the lithospheric mantle beneath the Ailaoshan segment. This comparison will be applied to explore distinct evolutionary history of lithospheric mantle beneath the Jinshajiang-Ailaoshan Ocean.

2. Geological background and sampling

The Jinshajiang ophiolite belt exposed within the N-S striking orogenic belt in the Sanjiang area, Southwest China (Mo et al., 1998; Wang et al., 2000a), represents an important branch of the Paleo-Tethys (Jian et al., 2009a, 2009b; Wang et al., 2018; Hu et al., 2019). It is located between the Qamdo-Simao and Zhongza blocks (Fig. 1). The Qamdo-Simao block has a ~ 1.44 Ga metamorphic basement represented by the Chongshan and Damenglong complexes (Zhong, 1998; Wang et al., 2000b, 2006). The Chongshan complex comprises gneiss, amphibolite, greywacke with interlayered phyllitic basic-intermediate meta-volcanics and bedded fine- or medium-grained marble (Wei et al., 1984; Wu et al., 1984), while the Damenglong complex is constituted by greenschists, meta-volcanics, greywacke, iron formation, amphibolite and associated granitoid intrusions (Yang et al., 1994). Ediacaran-Cambrian marine sediments which are common in the southeastern Yunnan province (Liu and Zhou, 2017) are missing in this area. Overlying the Proterozoic basements are the Lower Ordovician meta-strata, which consist of a sequence of slates, quartzites, phyllites and meta-limestones comparable with those of the Yangtze block. They are uncomfortably overlain by the Middle Devonian strata with basal conglomerates and shallow-marine sediments from bottom to top. The Carboniferous and Permian strata are shallow-marine and continental sequences with local coal lines, while the Triassic strata comprise clastics and carbonates (BGMRYP, 1990). Stratigraphic studies indicate that the Qamdo-Simao block once was part of the western Yangtze block before Middle Devonian, when the opening of the Ailaoshan Ocean separated them apart (Zhong, 1998; Wang et al., 2000a, 2006).

The Zhongza block has Lower Permian strata of massive limestones characterized by purple pelitic bands and fossils, which are similar to those of the Yangtze block. By contrast, sequences of the Upper Permian strata in the Zhongza block are featured by more input of submarine materials than those of the Yangtze block. Significantly, a set of massive basaltic flow with geochemical signature similar to the Emeishan flood basalts occurs between the Lower and Upper Permian strata (BGMRS, 1991). Stratigraphic and magmatic evidences support that the Zhongza block should have been connected with the Yangtze block before their separation in Permian, which responds to the initial opening of the Ganzi-Litang Ocean (Li et al., 2010).

Consumption of the Jinshajiang Ocean is characterized by the westward subduction of Jinshajiang oceanic crust beneath the Qamdo-Simao block (Zi et al., 2012a, b, c, 2013). The convergent process generated a continental margin arc zone, a collision-related volcano-sedimentary zone, an ophiolite mélange zone, and a foreland thrust and fold belt from west to east (Fig. 2; Zi et al., 2013). The continental margin arc occurs along the eastern margin of the Qamdo-Simao block. The collisional volcano-sedimentary zone is characterized by the Triassic turbidites and clastic sequences with associated bimodal volcanic rocks, which indicate an abyssal to bathyal environment (Mou and Wang, 2000; Tan, 2002). The Jinshajiang ophiolite mélange zone represents remnant of oceanic lithosphere of the Jinshajiang Ocean and is similar to the Ailaoshan ophiolite belt in the south (Wang et al., 2000a). The foreland thrust zone comprises series of west-verging structural slices, which

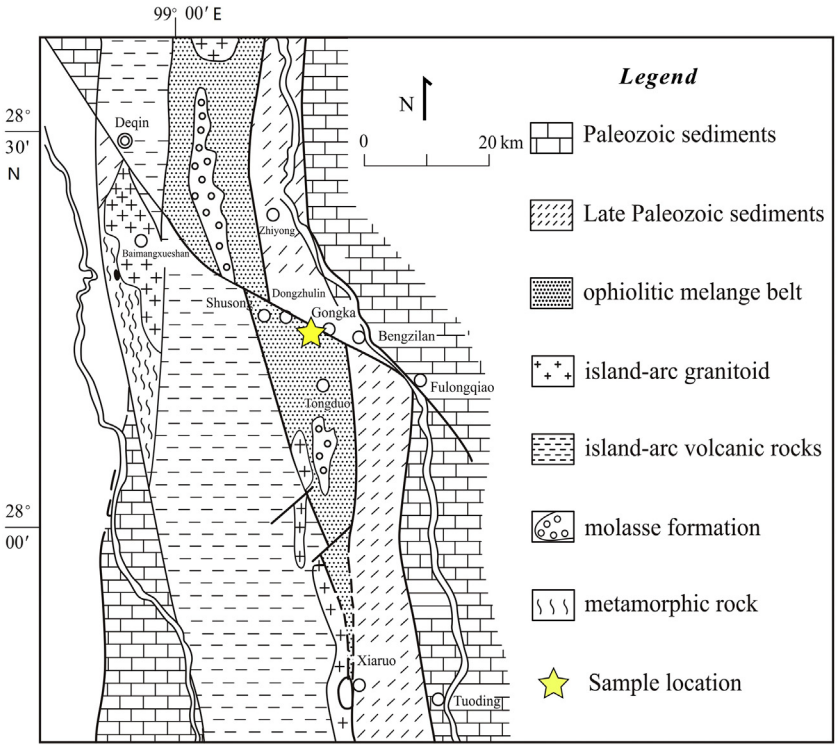

Fig. 2. Geological map of the Jinshajiang ophiolite belt (after Sun and Jian, 2004). Yellow star represents sampling location in this study.

crosscut the Devonian-Permian carbonates, turbidites and basalts of the passive margin of western Yangtze block (e.g., Leloup et al., 1995; Li et al., 2002).

The Jinshajiang ophiolite occurs along with the N–S striking Jinsha River over hundreds of kilometers (Fig. 2). It is constituted by blocks and/or olistoliths, which are entrained in a Middle Triassic turbiditic sequence and overlain by Late Triassic sandstones (Faure et al., 2016). Rocks of the ophiolite include dismembered peridotites, cumulate ultramafic-mafic rocks, volcanic lavas, and interlayered limestone and radiolarian chert (Mo et al., 1998; Wang et al., 2000a). The mantle peridotites occur as irregular veins, strip large-sized bodies (1 km across) or dismembered lenticular small-sized bodies (<100 m). They primarily comprise harzburgites with subordinate dunites, both of which have suffered large degrees of serpentinization. Cumulate ultramafic rocks are limitedly exposed and include harzburgites, dunites and pyroxenites, while the more abundant cumulate mafic rocks are featured by layered gabbros and anorthites (Wang, 1985; Jian et al., 2008). Field observation suggests that the former was separated from mantle peridotites by faults in the Xumai area (Mo et al., 1998). Pillow lavas are chemically basaltic and andesitic, and are widespread with typical pillow structure, chilled rim and radiated fractures, reflecting their eruption in a submarine environment (Wang, 1985). This study collected samples of mantle peridotites from the Dongzhulin area, where the ophiolite belt was eastward cut and slipped by a roughly E–W striking fault (Fig. 2). The sampled Jinshajiang peridotites are highly serpentinized. Olivines have been metasomatized to serpentines, chlorites and magnetites, whereas orthopyroxenes were altered to bastites. Cr-spinel grains are mostly subhedral to anhedral.

The Ailaoshan ophiolite on the southeast of the Jinshajiang ophiolite has similar lithological assemblages and deformation-metamorphic history (Fig. 1). Therefore, the two ophiolites were thought to be contiguous and represent different segments of the same ocean basin. Mantle peridotites from the Shuanggou area of the Ailaoshan ophiolite show great heterogeneity and may be derived from different processes and mantle domains (Hu et al., 2020). The Group-1 harzburgites from Hu et al. (2020) have whole rock compositions (e.g., major elements, PGE, and —Re–Os isotopes) comparable with abyssal peridotites; therefore, the Group-1 harzburgites represent the normal upper oceanic mantle of Paleo-Tethys, and their trace elements and mineral were also analyzed in this study for the purpose of comparison. Geological introduction and sample description of the Ailaoshan peridotites are referred to Hu et al. (2020).

3. Analytical methods

Major elemental compositions of spinel grains from the Jinshajiang and Ailaoshan peridotites were performed on a Link Energy Dispersive Spectrometry (EDS) System connected to a JEOL JXA-8230 electron probe micro-analyzer at the Department of Earth Sciences, the University of Hong Kong. Analytical conditions are in wavelength dispersive mode (WDS) with a 15 kV accelerating voltage, ~20 nA beam current, counting time of 10–20 s, and 1 μm beam diameter (Liu et al., 2019b). An internal spinel standard during interval of 10 sample analyses was measured to detect instrumental drift. The analytical uncertainties were < 2%.

Whole-rock major oxide concentrations for the Jinshajiang peridotites were determined by using a ME-XRF 06 spectrometer with relative standard deviation lower than 5% at the ALS laboratory. Trace elements were measured using an inductively coupled plasma mass spectrometry (ICP-MS) at the State Key Laboratory of Ore Deposit Geochemistry, Chinese Academy of Sciences (SKLODG). Trace elements were preconcentrated following the procedure of Qi et al. (2000). About 50 mg sample powder was digested with HF and HNO_3 mixture in a Teflon bomb, protected by a stainless-steel container, at ~190 °C for 48 h. Rhodium was used as an internal standard. International reference materials (BHVO-2 and BCR-2) were applied to control analytical quality. This method has an analytical precision about 10%. More details of procedure are referred to Qi et al. (2000).

Whole-rock platinum-group elements for the Jinshajiang peridotites were determined at SKLODG following procedure of Qi et al. (2011). Eight grams of sample powder along with the calculated isotope spikes (^{101}Ru, ^{193}Ir, ^{105}Pd and ^{194}Pt) were placed in a 120 mL PTFE beaker. 15–30 mL HF was added and evaporated to remove the silicates. The dried residue was dissolved with HF and HNO_3, sealed in a bomb and then heated to 190 °C for 48 h. PGE was pre-concentrated using co-precipitation along with Te. Te-precipitate was dissolved with diluted aqua regia and then loaded on a mixed ion exchange column (a Dowex 50 W X8 cation exchange resin and a P507 levextrel resin) to remove interfering elements (such as Cu, Ni, Zr and Hf). Analysis was performed on an isotope dilution ICP-MS at the SKLODG. The total procedural blanks were lower than 0.002 ppb for Ir, Rh and Pt, 0.012 ppb for Ru and 0.040 ppb for Pd. Quality-monitoring standard reference materials WGB-1 (gabbro) and WPR-1 (peridotite) yield results consistent with the recommended values (Qi et al., 2011).

Procedure of whole-rock Re–Os isotopes for the Jinshajiang peridotites follows that described by Chu et al. (2009). Two grams of sample powder were mixed with ^{187}Re–^{190}Os spike and then digested by reverse aqua regia in a Carius Tube at 240 °C for 72 h. Osmium was extracted from aqua regia solution by CCl_4 (Cohen and Waters, 1996) and further purified by micro-distillation (Birck et al., 1997). Rhenium was then recovered from the remained aqua regia solution using anion exchange chromatography with about 0.6 mL resin (AG 1 × 8, 100–200 mesh). Osmium isotopic compositions were performed on a GV Isoprobe-T Mass Spectrometer at the State Key Laboratory of Lithospheric Evolution, Institute of Geology and Geophysics, Chinese Academy of Sciences (IGGCAS). The measurement was carried out in static mode using nine Faraday cups. $Ba(OH)_2$ was used as an ion emitter to enhance the ionization efficiency. The Os isotopic compositions and Os concentrations were obtained in one mass spectrometric run. The measured Os isotopic ratios were corrected for mass fractionation using $^{192}Os/^{188}Os = 3.08271$ after interference corrections, oxygen corrections and spike subtractions. Osmium isotopic measurements have in-run precisions better than ±0.2% (2σ). Repeated measurements of the UMD Johnson-Matthey standard solution yielded $^{187}Os/^{188}Os$ ratio of 0.11380 ± 4 (2σ, $n = 5$). On the other hand, rhenium determination was conducted on a Neptune MC-ICP-MS using a secondary electron multiplier in peak-jumping mode. The in-run precisions were better than ± 0.5% (2σ) for Re analysis. Total analytical blanks were 2 pg for Re and 3–5 pg for Os with an $^{187}Os/^{188}Os$ ratio near 0.160. Repeated measurements of standard material WPR-1 obtained values identical to the recommended values.

4. Analytical results

4.1. Mineral compositions

Major elemental compositions of spinel grains in the Jinshajiang and Ailaoshan peridotites are supplied in Table S1. Spinel grains from the Jinshajiang peridotites have Cr# (Cr# = molar Cr/(Cr + Al)) values ranging from 0.42 to 0.60 and Mg# (Mg# = molar Mg/(Mg + Fe)) ratios of 0.60–0.71 with TiO_2 < 0.2 wt.%, FeO of 14.1–17.6 wt.% Cr_2O_3 of 35.2–46.7 wt.%, and Al_2O_3 of 21.2–33.4 wt.% (Table S1; Fig. 3). Spinel grains in the Ailaoshan peridotites have comparable Cr# from 0.37 to 0.57 and Mg# from 0.47 to 0.71.

4.2. Whole-rock major and trace elements

Whole-rock major oxide and trace elemental compositions are given in Table 1. In comparison with the Ailaoshan peridotites (SiO_2: 38.3–41.4 wt.%; MgO: 36.2–37.2 wt.%; Al_2O_3: 1.17–2.61 wt.%), the Jinshajiang peridotites have similar SiO_2 contents (36.0–39.7 wt.%), but slightly higher MgO contents (32.7–38.1 wt.%) and obviously

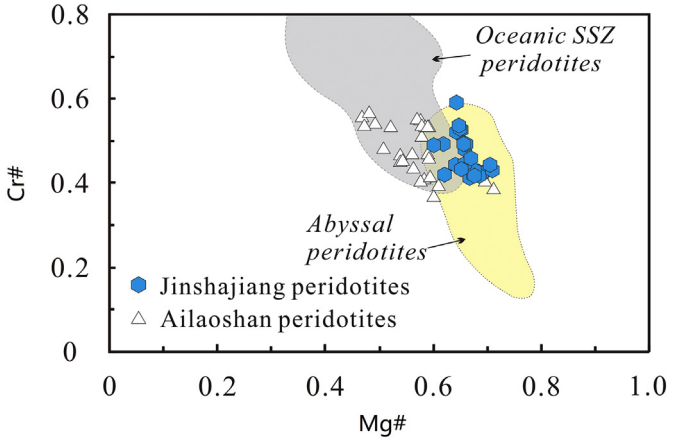

Fig. 3. Cr# vs. Mg# of spinels of the Jinshajiang and Ailaoshan peridotites. Data sources: abyssal peridotites (Dick and Bullen, 1984) and supra-subduction zone (SSZ) peridotites (Ishii et al., 1992; Parkinson and Pearce, 1998; Pearce et al., 2000).

lower Al_2O_3 contents (0.67–1.30 wt.%) (Table 1; Fig. 4). In the diagram of Al_2O_3/SiO_2 vs. MgO/SiO_2 (Fig. 4a), the Jinshajiang peridotites plot within the range of abyssal peridotites (Niu, 2004), but slightly below the "terrestrial array" (Hart and Zindler, 1986), indicating that MgO might be lost from the peridotites but Al_2O_3 was immobile during serpentinization. REE concentrations in the Jinshajiang peridotites are low (total REE = 0.37–1.28 ppm) with U-shaped chondrite-normalized patterns (Fig. 5). In comparison, the Ailaoshan peridotites have slightly higher REE concentrations (total REE = 0.63–3.38 ppm) accompanying with variable U-shaped REE patterns.

4.3. Whole-rock PGE compositions and —Re–Os isotopes

Whole-rock PGE compositions and $^{187}Os/^{188}Os$ ratios for the Jinshajiang peridotites are listed in Table 2. The Jinshajiang peridotites have PGE abundances comparable to the primitive upper mantle (PUM). Specifically, their PGE concentrations are 2.99–6.71 ppb for Os, 2.76–4.24 ppb for Ir, 6.11–10.2 ppb for Ru, 0.95–1.19 ppb for Rh, 3.87–11.8 ppb for Pt, and 4.59–10.5 ppb for Pd. They are characterized by overall flat PUM normalized PGE patterns (Fig. 6) with variable $(Os/Ir)_N$ and $(Pd/Ir)_N$ values of 0.77–2.18 and 0.61–1.66, respectively. Rhenium concentrations in the Jinshajiang peridotites are very low, varying from 0.06 ppb to 0.31 ppb, with a $^{187}Re/^{188}Os$ ratio range of 0.01–0.25. The Jinshajiang peridotites have highly variable $^{187}Os/^{188}Os$ values with range of 0.1272–0.1374, mostly higher than that of normal abyssal peridotites at given $^{187}Re/^{188}Os$ ratios (Fig. 7). One sample has $^{187}Os/^{188}Os$ value of 0.1374, even much higher than the recommended value of the PUM ($^{187}Os/^{188}Os = 0.1296 \pm 6$; Meisel et al., 2001). For the Carboniferous Jinshajiang ophiolite, accumulation of the daughter isotope after the formation of the oceanic lithosphere cannot account for the radiogenic isotope composition (Fig. 7). Initial $^{187}Os/^{188}Os$ values calculated at 343.5 Ma (zircon ages of gabbros in the Jinshajiang ophiolites; Jian et al., 2009b) vary from 0.1268 to 0.1361, which are still suprachondritic and correspond to $\gamma_{Os}(t)$ from 1.7 to 9.1. Whole-rock PGE compositions and Re–Os isotopes of the Ailaoshan peridotites have been reported in Hu et al. (2020). The selected Ailaoshan peridotites, i.e., the Group-1 harzburgites in Hu et al. (2020), are characterized by PGE patterns and $^{187}Os/^{188}Os$ ratios (0.1230–0.1273) similar to those of abyssal peridotites, and in turn are proposed to be representative of the normal lithospheric mantle beneath the Ailaoshan segment (Figs. 6 and 7).

Table 1
Major oxide and trace element compositions of peridotites from the Jinshajiang and Ailaoshan ophiolites.

Location	Jinshajiang					Ailaoshan[a]						
Sample No.	DQ1103	DQ1104	DQ1106	DQ1108	DQ1314	SG1111	SG1112	SG1313	SG1317	SG1328	SG1329	SG1330
Major elements determined by XRF (wt.%)												
SiO_2	38.7	38.2	36.0	38.4	39.7	38.7	38.3	39.2	41.4	39.1	38.9	39.0
Al_2O_3	0.74	1.16	0.67	1.11	1.30	2.03	2.61	1.64	1.17	1.47	2.44	2.61
Fe_2O_3	7.32	7.67	7.20	7.51	8.04	6.55	7.30	7.48	7.57	6.91	7.91	8.37
CaO	0.22	0.02	4.66	<0.01	0.11	0.51	0.02	0.03	0.31	0.46	0.13	0.02
MgO	38.1	37.4	32.7	37.8	36.8	37.0	36.7	37.2	35.8	37.4	36.2	36.2
Na_2O	<0.01	<0.01	<0.01	<0.01	0.04	<0.01	<0.01	0.05	0.05	0.06	0.05	0.05
K_2O	0.01	<0.01	0.01	0.01	0.04	0.01	0.02	<0.01	<0.01	<0.01	0.01	0.01
Cr_2O_3	0.32	0.40	0.45	0.35	0.38	0.31	0.37	0.32	0.39	0.41	0.36	0.34
TiO_2	0.01	0.01	0.01	<0.01	0.02	0.03	0.09	<0.01	<0.01	<0.01	0.05	0.08
MnO	0.03	0.09	0.05	0.09	0.08	0.07	0.09	0.11	0.07	0.09	0.07	0.06
P_2O_5	0.01	0.01	0.01	0.01	0.02	<0.01	<0.01	<0.01	0.01	<0.01	<0.01	<0.01
LOI	13.80	13.40	17.20	13.70	12.63	13.70	14.15	13.40	13.10	14.00	13.40	13.30
Total	99.29	98.31	99.00	98.93	99.18	98.86	99.63	99.48	99.82	99.86	99.59	100.06
Trace elements determined by ICP-MS (ppm)												
La	0.05	0.05	0.05	0.13	0.07	0.20	0.22	0.08	0.67	0.14	0.18	0.22
Ce	0.16	0.10	0.16	0.30	0.15	0.30	0.44	0.14	1.35	0.19	0.60	0.73
Pr	0.02	0.03	0.01	0.05	0.01	0.03	0.04	0.01	0.17	0.02	0.09	0.13
Nd	0.08	0.04	0.05	0.21	0.03	0.07	0.21	0.08	0.58	0.02	0.38	0.72
Sm	0.02	0.01	0.01	0.06	0.01	0.06	0.11	0.02	0.12	0.02	0.16	0.19
Eu	0.01	0.00	0.00	0.01	0.00	0.04	0.07	0.00	0.05	–	0.03	0.06
Gd	0.03	0.01	0.02	0.08	0.02	0.09	0.21	0.02	0.12	–	0.16	0.18
Tb	0.01	0.00	0.00	0.02	0.00	0.02	0.04	0.00	0.02	–	0.02	0.04
Dy	0.04	0.03	0.02	0.14	0.05	0.22	0.39	0.08	0.10	0.03	0.12	0.19
Ho	0.01	0.01	0.01	0.03	0.02	0.05	0.08	0.01	0.03	0.02	0.02	0.03
Er	0.03	0.03	0.02	0.11	0.04	0.14	0.25	0.08	0.06	0.06	0.05	0.07
Tm	0.01	0.01	0.00	0.01	0.01	0.03	0.03	0.01	0.01	0.01	0.01	0.01
Yb	0.04	0.06	0.03	0.11	0.06	0.20	0.25	0.08	0.09	0.07	0.05	0.05
Lu	0.01	0.01	0.01	0.02	0.01	0.03	0.05	0.02	0.02	0.02	0.01	0.01
Nb	0.07	0.03	0.08	0.09	0.12	0.09	0.22	0.08	1.76	0.11	0.13	0.19
Cu	20.7	4.07	23.7	7.55	16.6	10.1	4.82	8.69	0.88	1.04	11.4	11.4

[a] Data of major elements and Yb of for the Ailaoshan peridotites are from Hu et al. (2020).

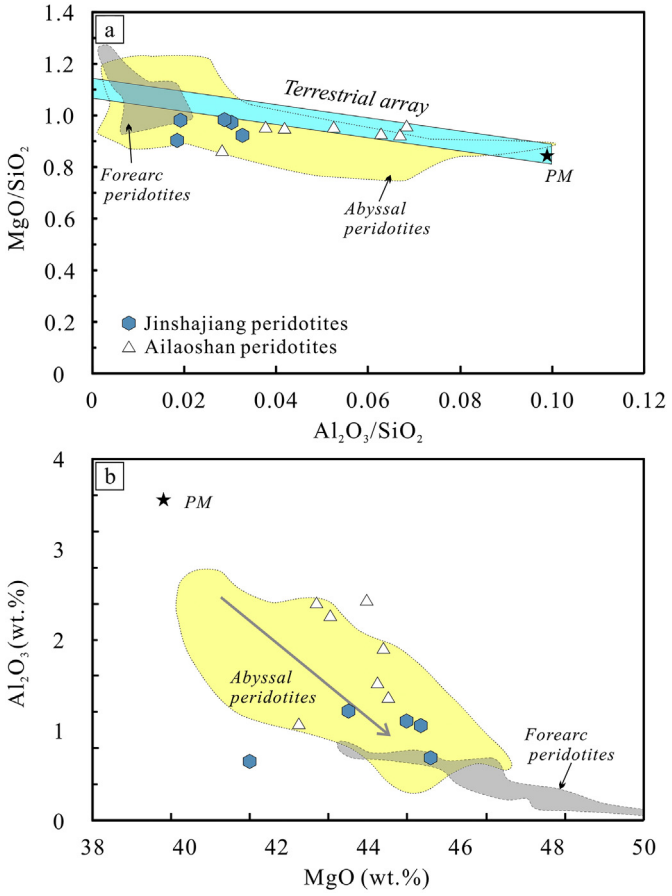

Fig. 4. (a) MgO/SiO_2 vs. Al_2O_3/SiO_2 and (b) Al_2O_3 vs. MgO diagrams for the Jinshajiang and Ailaoshan peridotites. Data of primitive mantle come from McDonough and Sun (1995). Data sources: forearc peridotites (Parkinson and Pearce, 1998), and the abyssal peridotites (Niu, 2004). The blue field in Fig. 4a represents 'Terrestrial array' (Hart and Zindler, 1986).

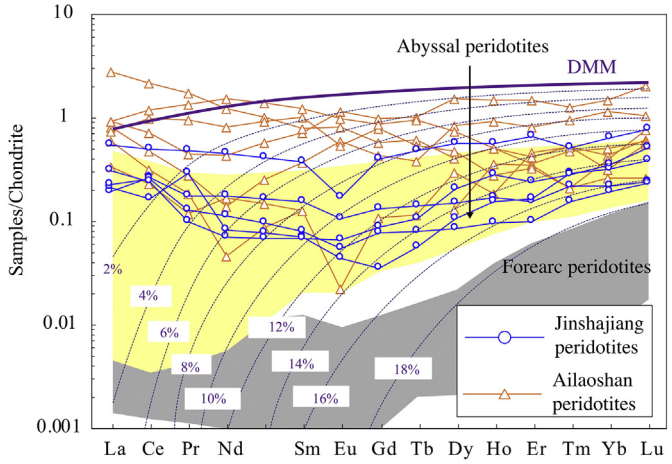

Fig. 5. Chondrite-normalized REE patterns for the Jinshajiang peridotites and the Ailaoshan peridotites. Normalized values are from Sun and McDonough (1989). The DMM compositions are from Workman and Hart (2005). Dashed lines represent non-modal fractional melting of DMM with 2% degree increments (Warren, 2016). Data source: abyssal peridotites (Niu, 2004) and forearc peridotites (Parkinson and Pearce, 1998).

5. Discussion

5.1. Tectonic setting of the Jinshajiang peridotites

Ophiolite sequences could be produced during almost every evolutional stage of oceanic basin, from continental rifting, seafloor spreading, oceanic plate consumption to final continental collision (Dilek and Furnes, 2011, 2014; Pearce, 2014). These rocks thus bear key information to reconstruct the evolution of oceanic basins (e.g., Miyashiro, 1973; Pearce and Robinson, 2010; Pearce, 2014). Typical crustal sequences within the Jinshajiang ophiolite belt preserve evidence for tracing the evolution of the Jinshajiang Ocean (Hu et al., 2019). Crustal rocks in the Zhiyong area were determined with U–Pb ages of 343.5 ± 2.7 Ma (Jian et al., 2008, 2009b), and show compositions similar to enriched mid-ocean-ridge basalts (E-MORB), indicating that they were formed in a spreading ridge of the ocean (Hu et al., 2019). In comparison, crustal sequence in the Baimaxueshan area was formed at 285–282 Ma (Jian et al., 2008) and have geochemically affinities with arc lavas (e.g., —Nb–Ta depletions and lower $\varepsilon_{Nd}(t)$ values). Further investigation indicates that the arc-like signatures reflect mantle source metasomatism by fluids dehydrated from the subducting slab rather than crustal assimilation processes en route (Hu et al., 2019). It is thus proposed that opening and closure of the Jinshajiang Ocean started at the Early Carboniferous and Early Permian, respectively (Hu et al., 2019; Zi et al., 2012b).

Mantle peridotites in this study were collected in the Dongzhulin area, associated with crustal sequences formed at the interval of 354–340 Ma: a trondjemite and a layered gabbro from the Dongzhulin ophiolite section yielded a similar zircon age of 347 ± 7 Ma and 354 ± 3 Ma, respectively (Wang et al., 2012; Zi et al., 2012b), and Wang et al. (2000a) reported a plagiogranite with a zircon age of 340 ± 3 Ma. These rocks have been ascribed to initial rifting or spreading of the Jinshajiang Ocean (Wang et al., 2000a, 2012; Zi et al., 2012b). Consequently, it is highly possible that the peridotites were also formed in the opening stage of the Jinshajiang Ocean (Zi et al., 2012b). This interpretation is further supported by whole-rock and mineral geochemistry of the peridotites as shown below.

(i) Addition of fluids into the mantle wedge would significantly decrease the melting temperature of mantle (Kushiro et al., 1968; Gaetani and Grove, 1998), further promoting partial melting in the mantle wedge (e.g., Schmidt and Poli, 1998; Grove et al., 2006). Therefore, the sub-arc mantle peridotites (e.g., Parkinson and Pearce, 1998) are generally more refractory than the abyssal peridotites (e.g., Niu, 2004). In terms of major compositions, the Jinshajiang peridotites are very similar to the abyssal peridotites, with higher Al_2O_3 and lower MgO contents than typical fore-arc peridotites (Fig. 4), indicating that the Jinshajiang peridotites in this study are not as refractory as those fore-arc peridotites.

(ii) A useful index of mantle melting is the Cr# values of spinel, which would increase with higher mantle melting. In the Jinshajiang peridotites, spinels show lower Cr# values than those in the fore-arc peridotites. Almost all the data are plotted in the area of spinels in the abyssal peridotites (Dick and Bullen, 1984) (Fig. 3). Melt percentage (F) could be further calculated with the function $F = 10 \times \ln(Cr\#) + 24$, which is valid for spinel with Cr# from 0.1 to 0.6 (Hellerbrand et al., 2001). Calculations based on compositions of spinel suggest that the Jinshajiang peridotites have undergone moderate degrees of partial melting (15%–20%), which are comparable with the abyssal peridotites.

(iii) MREE-HREEs can also be used to distinguish abyssal peridotites and subarc peridotites, as they are incompatible during mantle melting and relatively difficult to be modified by processes after the melting. As shown in Fig. 5, sub-arc mantle peridotites have lower HREE concentrations due to the larger degrees of melting (Parkinson and Pearce, 1998; Niu, 2004). The feature of relatively high HREE contents in the Jinshajiang peridotites is indicative of a mantle source without replicated melt extractions like that for sub-arc mantle (Fig. 5). Model of partial melting process based on the HREE and MREE variations confirms about 8%–16% melt extraction from a depleted MORB source for the

Table 2
PGE and —Re–Os isotopic compositions of peridotites from the Jinshajiang ophiolite.

Sample No.	Os (ppb)	Ir (ppb)	Ru (ppb)	Rh (ppb)	Pt (ppb)	Pd (ppb)	Re (ppb)	$^{187}Re/^{188}Os$	$^{187}Os/^{188}Os$	$(^{187}Os/^{188}Os)_i$[a]
DQ1103	6.71	2.76	7.51	0.95	3.87	6.59	0.312	0.225	0.1374	0.1361
DQ1104	3.77	4.24	10.2	1.19	9.33	7.74	0.055	0.070	0.1272	0.1268
DQ1106	2.99	3.50	8.61	1.12	11.1	9.75	0.155	0.250	0.1307	0.1293
DQ1106-R[b]	3.17	3.12	8.14	1.23	11.8	10.5	0.167	0.269	0.1308	0.1293
DQ1108	4.30	3.69	8.46	0.98	6.75	5.97	0.072	0.081	0.1285	0.1281
DQ1108-R	4.23	3.41	8.26	0.99	6.92	6.17	0.090	0.103	0.1278	0.1272
DQ1314	3.22	3.68	6.11	1.17	4.87	4.59	0.068	0.102	0.1286	0.1280

[a] Initial $^{187}Os/^{188}Os$ compositions are calculated at the age of 343.5 Ma for the Jinshajiang peridotites (Jian et al., 2009b).
[b] Replicate analysis.

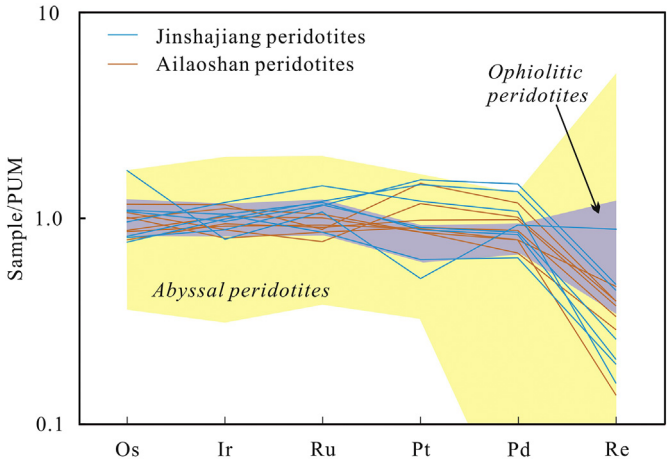

Fig. 6. Primitive upper mantle (PUM)-normalized PGE diagrams for the Jinshajiang peridotites. Compositions of the PUM are from Becker et al. (2006) and Fischer-Gödde et al. (2011). Data of the Ailaoshan peridotites are from Hu et al. (2020). Data of the ophiolitic peridotites are from Becker et al. (2006) and Fischer-Gödde et al. (2011), while data of abyssal peridotites are after the compilation by Day et al. (2017) (three highly fractionated samples are excluded).

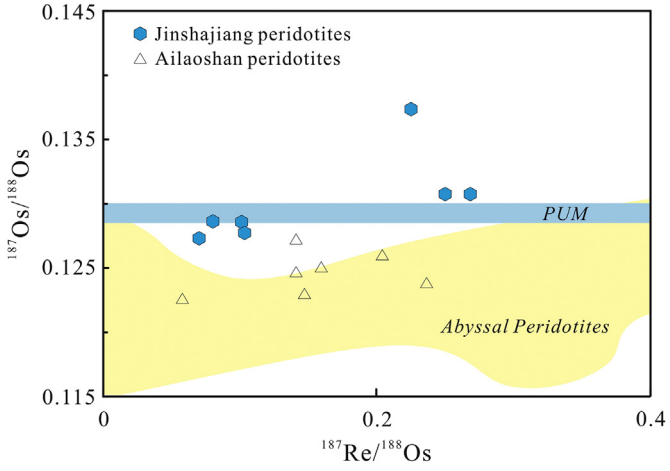

Fig. 7. Re–Os isotopic compositions of the Jinshajiang peridotites. Data of the Ailaoshan peridotites are from Hu et al. (2020). $^{187}Os/^{188}Os$ of PUM come from Meisel et al. (2001). The field of abyssal peridotite is after abyssal peridotite data from Brandon et al. (2000), Alard et al. (2005), Harvey et al. (2006), and Liu et al. (2008).

Jinshajiang peridotites (Fig. 5), similar to the results of spinel. Therefore, the above evidences suggest that the Jinshajiang peridotites in this study are comparable with the abyssal peridotites which are produced in the opening stage of the ocean.

5.2. Melt-rock reaction after mantle melting

The above discussion indicates that the Jinshajiang peridotites are residues after moderate degrees of melt extraction. However, partial melting process cannot produce the LREE enrichments relative to MREE and HREE in the Jinshajiang peridotites. Processes after mantle melting must exist to result in the U-shaped REE patterns of the Jinshajiang peridotites. Possible mechanisms include (1) hydrothermal processes as evidenced by serpentinization (e.g., Gruau et al., 1998), and (2) mantle metasomatism such as refertilization and melt-rock reaction (Zhou et al., 2005). It has been proposed that these processes can be distinguished by trace elements of different mobilities in fluids (Paulick et al., 2006): LREE are more readily transported than HREE and high field strength elements (HFSE) in hydrothermal fluids, whereas both REE and HFSE can be added into the mantle peridotites through percolation of melts (e.g., refertilization and melt-rock reaction) (Niu, 2004; Paulick et al., 2006). However, correlations of different elements of the Jinshajiang peridotites were hardly distinguished from trends defined by these different processes (Fig. 8), indicating that the lithophile elements are insufficient to discriminate these processes in this study.

Platinum group elements (PGEs), as a coherent group of highly siderophile elements (HSEs), are mainly hosted in accessory base-metal sulfides (BMS) in mantle peridotites (Barnes et al., 1985; Alard et al., 2000; Mungall and Naldrett, 2008; Lorand et al., 2013) and have shown huge potential in providing details about processes in the upper mantle, relative to traditionally incompatible lithophile elements (Lorand et al., 2008). Available knowledge of PGE suggests that mantle melting would cause systematical PPGE (Palladium-group PGE: Pt, Pd, and Rh) depletion relative to IPGE (Iridium-group PGE: Os, Ir, and Ru) in the residue by removing Pd-Cu-Ni rich sulfides (Lorand et al., 2008, 2013). However, in the case of the Jinshajiang peridotites, $(Pd/Ir)_N$ ratios and Pd concentrations increase with the decrease of Al_2O_3 (Fig. 9), contrary to the expectation of mantle melting process during which both Al_2O_3 and PPGE are removed from the source.

During mantle melting, Re behaves as a moderately incompatible trace element with a bulk coefficient similar to aluminum, while Os is highly compatible. Melt extraction would produce low Re/Os ratios and consequently limit the growth of $^{187}Os/^{188}Os$ in the residue. After a short time, residue of high degree of melting would have low Al_2O_3 contents and slightly low $^{187}Os/^{188}Os$ ratios relative to residue of low degree of melting. But after a long time, residue of large degree of melting would have not only lower Al_2O_3 contents but also much lower $^{187}Os/^{188}Os$ than residue of low degree of melting. The Carboniferous Jinshajiang ophiolite is a young ophiolite, a slightly positive correlation between $^{187}Os/^{188}Os$ ratios and Al_2O_3 contents is expected if the Jinshajiang peridotites was only controlled by mantle melting. However, the Jinshajiang peridotites have comparable or higher $^{187}Os/^{188}Os$ ratios (0.1272–0.1374) than the inferred primitive mantle ($^{187}Os/^{188}Os = 0.1296 \pm 6$; Meisel et al., 2001). Moreover, the $^{187}Os/^{188}Os$ ratios show negative correlations with Al_2O_3 contents, contrary to the predicted trend of mantle melting (Fig. 9c). Therefore, a

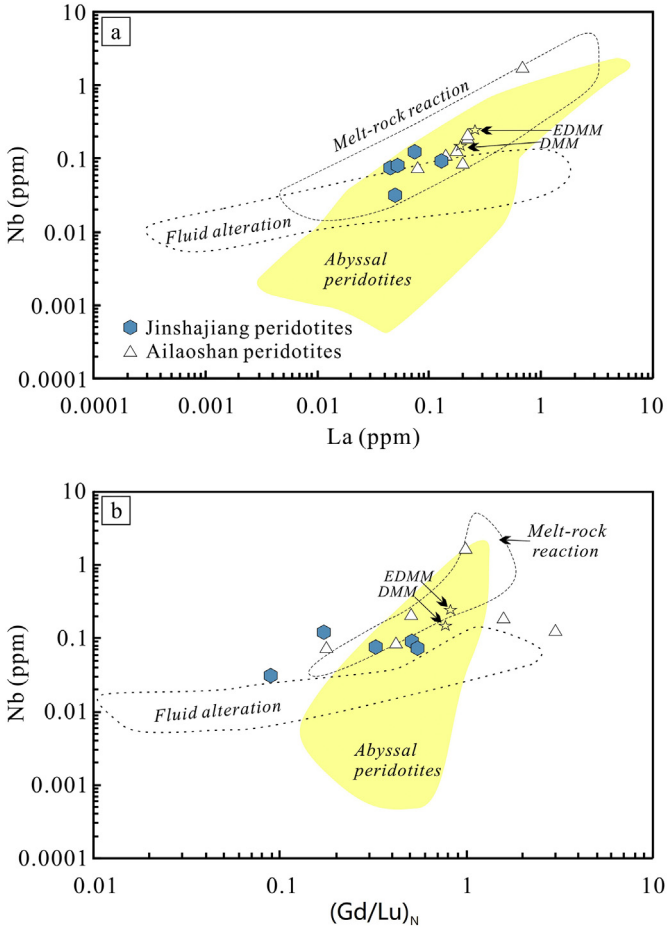

Fig. 8. Correlations of Nb with La (a) and Gd/Lu_N (b) for the Jinshajiang and Ailaoshan peridotites. Data of DMM and EDMM come from Workman and Hart (2005). Trends of fluid alterations and melt-rock reaction were defined by the Mid-Atlantic peridotites (Paulick et al., 2006).

secondary process after melt extraction is required to explain the systematical change of PGE and Re–Os features in the Jinshajiang peridotites.

Previous studies proposed that the PGE abundances and Re–Os isotopic system in mantle peridotites after melt extraction can be overprinted by (i) hydrothermal processes (e.g., serpentinization) and (ii) mantle metasomatism (e.g., refertilization and melt-rock reaction) (Lorand et al., 2013; Rudnick and Walker, 2009). To date, it is widely accepted that the serpentinization process has little influence on HSEs (Burnham et al., 1998; Harvey et al., 2006; Chen and Xia, 2008; Schulte et al., 2009; Dai et al., 2011; O'Driscoll et al., 2012) because the reducing conditions in the process tend to stabilize HSE-bearing mineral phases (Snow and Reisberg, 1995; Buchl et al., 2002; Hyndman and Peacock, 2003; Mével, 2003; Evans et al., 2013). By contrast, whether the serpentinization process would enrich Re concentrations is still in hot debate (e.g., Harvey et al., 2006; Liu et al., 2008). For the Jinshajiang peridotites, both the relative low contents of Re (0.06–0.31 ppb) and its negative correlation with Al_2O_3 indicate that the Re budget in the Jinshajiang peridotites are mainly controlled by magmatic processes (Fig. 9d).

Mantle metasomatism by percolation of melts can be categorized into two processes, i.e., mantle refertilization and melt-rock reaction (Rudnick and Walker, 2009; Liu et al., 2010a). Mantle refertilization refers to the process that transforms the original refractory peridotites like harzburgites into lherzolites via addition of silicate melts (e.g., Le Roux et al., 2007). Because mantle-derived melts are generally enriched in Re and PPGE relative to IPGE, refertilization can lead to increase of $(Pd/Ir)_N$ and $^{187}Os/^{188}Os$ together with the increase of Al_2O_3 (Rudnick and Walker, 2009; Lorand et al., 2013). However, the Jinshajiang peridotites exhibit negative correlations between Al_2O_3 and $(Pd/Ir)_N$ as well as $^{187}Os/^{188}Os$ (Fig. 9), indicating that the PGE budget and Re–Os isotopes are not controlled by the mantle refertilization process.

The melt-rock reaction refers to open-system interaction between silicate melts and peridotitic mantle (Rudnick and Walker, 2009). In the abyssal peridotites, silicate melts passing through the oceanic lithosphere commonly consume mantle pyroxenes and precipitate olivines (Kelemen, 1990; Kelemen et al., 1992, 1995, 1997). The resultant peridotites would be more refractory (e.g., decrease in Al_2O_3), and their PGE abundances and —Re–Os isotope systems could be strongly modified due to sulfide redistribution during the melt-rock reaction (e.g., Buchl et al., 2002; Xiong et al., 2020). For instance, Buchl et al. (2002) identified a systematic increase of Pd/Ir and $^{187}Os/^{188}Os$ from the harzburgite to the dunite vein on a single melt channel from the Troodos Ophiolite Complex. In their case, the dunite vein was formed by percolation of S-unsaturated melt at large melt/rock ratios, during which sulfides in the peridotites were dissolved by the percolating melt. In turn, this process led the PGE abundances of the dunites towards those of typical melts, i.e., much lower PGE concentrations than the PUM and enrichment in PPGE relative to IPGE. However, the Jinshajiang peridotites have PGE concentrations similar to PUM (Fig. 6) and variable Pd/Ir ratios ranging from values below the PUM to values above the PUM (Fig. 9) (Becker et al., 2006; Fischer-Gödde et al., 2011), contrary to the model of S-unsaturated melt percolation (Buchl et al., 2002). Instead, a model of sulfide addition by percolation of S-saturated melts is more reasonable (Xu et al., 2020). On the one hand, during the melt-rock interaction, the melts made the peridotites more refractory in terms of major compositions (e.g., decrease of Al_2O_3 contents). On the other hand, sulfide can be precipitated from the S-saturated melts, resulting in enrichment of PPGE relative to IPGE (Fig. 9a). The two samples (DQ1103 and DQ1106) with highest $(Pd/Ir)_N$ ratios (≥1.18) also have high Cu contents (20.7–23.7 ppm), which are also consistent with this model (Xu et al., 2020).

5.3. Comparison between the Jinshajiang and Ailaoshan peridotites

Regionally, the Ailaoshan ophiolite belt is comparable with the Jinshajiang ophiolite belt in terms of lithological assemblages and deformation-metamorphic history. Thus, these two ophiolite belts were considered to be continuous and mark the same ocean, i.e., the Jinshajiang-Ailaoshan Ocean (e.g., Wang et al., 2000a). Despite the previously proposed similarities, remarkable differences between these belts have also been identified, including (i) the diachronous opening of the Jinshajiang-Ailaoshan Oceans, that the Ailaoshan segment opened at ~380 Ma, followed by opening of the Jinshajiang segment at ~340 Ma (Zhong, 1998; Wang et al., 2000a; Jian et al., 2009b); (ii) contrasting characteristics of rifted margins for the Jinshajiang and Ailaoshan segments, that the Ailaoshan ophiolite is accompanied by a non-volcanic rifted margin whereas the Jinshajiang segment is associated with a volcanic rifted margin (Xiao et al., 2008; Jian et al., 2009b); and (iii) distinct geochemistry of oceanic crust within these belts, that the oceanic crust in the Ailaoshan ophiolite is similar to N-MORB whereas the Jinshajiang oceanic crust is comparable with E-MORB (Hu et al., 2015, 2019).

This study allows further comparison of lithospheric mantle between the Jinshajiang and Ailaoshan ophiolites. Within the Ailaoshan ophiolite belt, the Shuanggou ophiolite is the best-preserved part; the Shuanggou ophiolite is characterized by a lherzolite-dominated mantle sequence and a smaller mafic crustal sequence without sheeted dykes. These features are comparable with ophiolites formed at continental margins or slow spreading ridges (Pamić et al., 2002; Schaltegger et al., 2002; Montanini et al., 2008). The Ailaoshan peridotites selected in this study are from the Shuanggou area and exhibit PGE patterns and $^{187}Os/^{188}Os$ ratios (0.1230–0.1273) similar to those of oceanic

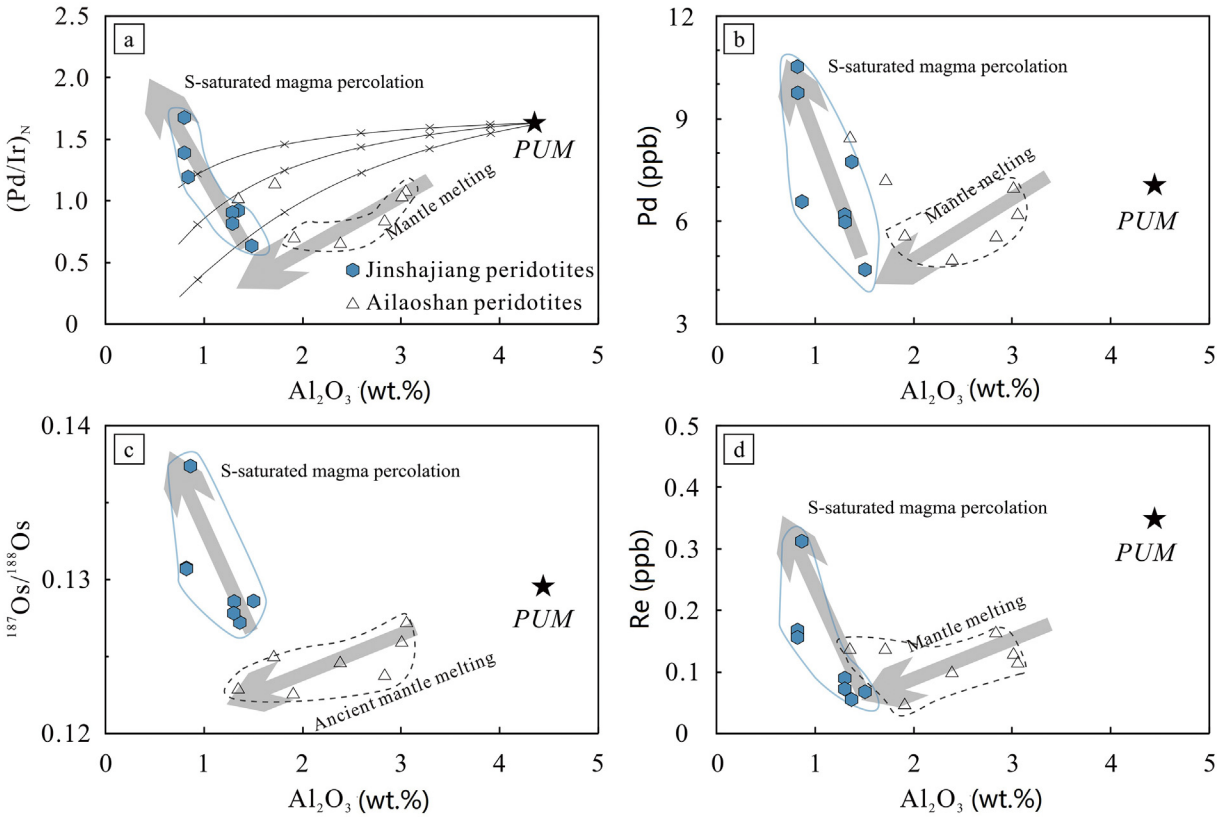

Fig. 9. Correlations of Al_2O_3 with $(Pd/Ir)_N$ (a), Pd (b), $^{187}Os/^{188}Os$ (c) and Re (d) in the Jinshajiang and Ailaoshan peridotites. PGE compositions of the PUM are from Becker et al. (2006) and Fischer-Gödde et al. (2011), whereas $^{187}Os/^{188}Os$ of the PUM is from Meisel et al. (2001). Curves in Fig. 9a represent fractional melting trends with different partition coefficients of Pd and Ir between sulfide and silicate melt after the model of Xu et al. (2020). Tick marks are with 5% melting increments.

peridotites (Figs. 6 and 9), indicating that these peridotites can represent the lithospheric mantle beneath the spreading center of the Ailaoshan segment (Hu et al., 2020).

The Jinshajiang peridotites are more refractory than the Ailaoshan peridotites in terms of whole-rock major compositions, as evidenced by their lower Al_2O_3 contents (Fig. 4). This could be explained by larger degrees of melting in the Jinshajiang peridotites than in the Ailaoshan peridotites. However, spinels in the Jinshajiang peridotites have Cr# (0.42–0.60) similar to spinels in the Ailaoshan peridotites (0.37–0.57), indicating comparable moderate degrees of partial melting for both the Jinshajiang and Ailaoshan peridotites (Table S1). Moreover, most of Ailaoshan peridotites (except for two samples with higher HREE contents) exhibit HREE patterns similar to Jinshajiang peridotites (Fig. 5). From this perspective, we consider that peridotites from the Jinshajiang and Ailaoshan ophiolites have experienced similar degrees of melt extraction.

As discussed before, the low Al_2O_3 contents in the Jinshajiang peridotites tend to reflect the melt-rock reaction processes after melting. The Jinshajiang peridotites have $^{187}Os/^{188}Os$ isotopes more radiogenic than the Ailaoshan peridotites (Fig. 7). In the Ailaoshan peridotites, most $(Pd/Ir)_N$ ratios and Pd concentrations decrease with the decrease of Al_2O_3, indicating that the Ailaoshan peridotites are mainly controlled by the melting processes and did not suffer any significant modification by melts (Fig. 9). On the other hand, two Ailaoshan peridotites have higher Pd concentrations and $(Pd/Ir)_N$ ratios, which could be explained by either PPGE-rich sulfide addition during melt percolation or local re-precipitation of PPGE-sulfide during melting. However, these two samples have $^{187}Os/^{188}Os$ ratios similar to the other Ailaoshan peridotites; this indicates that, for the model of melt percolation, the melt should have $^{187}Os/^{188}Os$ ratios comparable to the peridotites.

Whether melt-rock reaction would change Os isotopic features of mantle peridotites depend on the nature of percolating melts (Buchl et al., 2002; Xu et al., 2020). For instance, percolation of boninitic melts could cause an increase of $^{187}Os/^{188}Os$ ratio in peridotites of the Troodos Ophiolite Complex (Buchl et al., 2002), while percolation of forearc basaltic melts hardly changed Os isotope compositions in the Yarlung-Zangbo ophiolitic peridotites (Xu et al., 2020). For the Jinshajiang peridotites, it is clear that samples with high $(Pd/Ir)_N$ ratios show coupled elevated $^{187}Os/^{188}Os$ (Fig. 9), indicating that the later percolating magma must have high $^{187}Os/^{188}Os$ ratios. The Jinshajiang ophiolite is associated with a volcanic-rifted margin where OIB-type basaltic rocks were identified (Zhang et al., 1996; Xiao et al., 2008; Jian et al., 2009b); consequently, it has been proposed that the rifting mechanism of the Jinshajiang segment was strongly related to a Paleo-Tethys plume (Xiao et al., 2008). However, it seems unlikely that the OIB-like magmas have directly reacted with the Jinshajiang peridotites because they are generally sulfur-unsaturated. Indeed, E-MORB-like oceanic crusts have been widely reported in the Jinshajiang ophiolite (e.g., Jian et al., 2009b), indicating that the asthenosphere beneath the spreading ridge could have been affected by the plumes (e.g., Le Roux et al., 2002; Cushman et al., 2004). Magma from the modified asthenosphere is not only S-saturated but also has high radiogenic isotope compositions (Hu et al., 2019). The E-MORB magma is therefore a suitable candidate for the later percolating magma which has modified the Jinshajiang peridotites. By contrast, no evidence supports a similar scenario for the Ailaoshan peridotites (Fig. 10), as these peridotites are associated with N-MORB oceanic crust (Hu et al., 2015) and the Ailaoshan ophiolite was combined with a non-volcanic margin (Jian et al., 2009b).

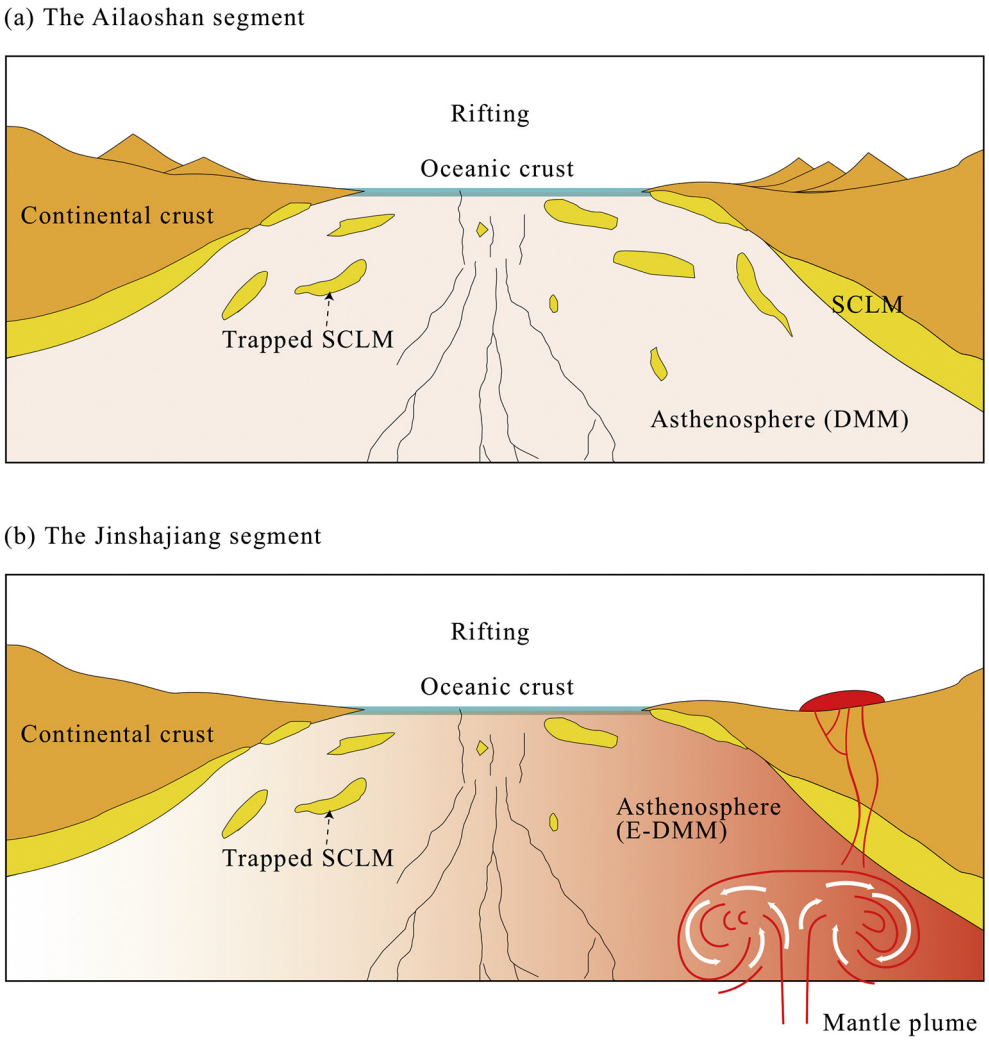

Fig. 10. A cartoon showing the contrasting rifting mechanisms between the Ailaoshan (a) and Jinshajiang (b) segments during the opening of the Jinshajiang-Ailaoshan Ocean.

6. Conclusions

Whole-rock and spinel compositions indicate that the Jinshajiang peridotites were generated in the spreading middle ridge of the Jinshajiang segment of the eastern Paleo-Tethys. They are residues after moderate degrees of melt extraction and have experienced percolation of sulfur-saturated melts, which were derived from an ^{187}Os-enriched mantle domain. Regional comparison between peridotites in the Ailaoshan and Jinshajiang ophiolites reveals considerable heterogeneity in the lithospheric mantle of the eastern Paleo-Tethys.

Declaration of Competing Interest

The authors declare that they have no known competing financial interests or personal relationships that could have appeared to influence the work reported in this paper.

Acknowledgments

The authors appreciate the assistance of Jing Hu, Yifan Yin and Yan Huang with major elements at the SKLODG, and the help of Zhuyin Chu, Junjie Xu, and Huihui Cao with Re–Os isotopic analysis. We are grateful to Fu Xiao who kindly provided help on EPMA analysis. Helpful and constructive comments from the Associate Editor Dr. Kristoffer Szilas, Dr. Jingao Liu and an anonymous reviewer are gratefully acknowledged. This study was financially supported by the National Natural Science Foundation of China (Grant No. 41425011).

Appendix A. Supplementary data

Supplementary data to this article can be found online at https://doi.org/10.1016/j.gsf.2020.11.011.

References

Alard, O., Griffin, W.L., Lorand, J.P., Jackson, S.E., O'Reilly, S.Y., 2000. Non-chondritic distribution of the highly siderophile elements in mantle sulphides. Nature 407, 891–894.

Alard, O., Luguet, A., Pearson, N.J., Griffin, W.L., Lorand, J.P., Gannoun, A., Burton, K.W., O'Reilly, S.Y., 2005. In situ Os isotopes in abyssal peridotites bridge the isotopic gap between MORBs and their source mantle. Nature 436, 1005–1008.

Barnes, S.J., Naldrett, A.J., Gorton, M.P., 1985. The Origin of the Fractionation of Platinum-Group elements in Terrestrial Magmas. Chem. Geol. 53, 303–323.

Becker, H., Horan, M.F., Walker, R.J., Gao, S., Lorand, J.P., Rudnick, R.L., 2006. Highly siderophile element composition of the Earth's primitive upper mantle: Constraints from new data on peridotite massifs and xenoliths. Geochim. Cosmochim. Acta 70, 4528–4550.

Birck, J.L., Barman, M.R., Capmas, F., 1997. Re-Os Isotopic Measurements at the Femtomole Level in Natural Samples. Geostand. Newslett. 21, 19–27.

Bodinier, J.L., Godard, M., 2003. Orogenic, ophiolitic, and abyssal peridotites. Treat. Geochem. 2, 568.

Brandon, A.D., Snow, J.E., Walker, R.J., Morgan, J.W., Mock, T.D., 2000. ^{190}Pt–^{186}Os and ^{187}Re–^{187}Os systematics of abyssal peridotites. Earth Planet. Sci. Lett. 177, 319–335.

Buchl, A., Brugmann, G., Batanova, V.G., Munker, C., Hofmann, A.W., 2002. Melt percolation monitored by Os isotopes and HSE abundances: a case study from the mantle section of the Troodos Ophiolite. Earth Planet. Sci. Lett. 204, 385–402.

Bureau of Geology and Mineral Resources of Sichuan Province (BGMRS), 1991. Regional Geology of Sichuan Province. Geological Publishing House, Beijing, p. 728 (in Chinese).

Bureau of Geology and Mineral Resources of Yunnan Province (BGMRYP), 1990. Regional Geology of Yunnan Province. Geological Publishing House, Beijing, p. 728 (in Chinese).

Burnham, O., Rogers, N., Pearson, D., Van Calsteren, P., Hawkesworth, C., 1998. The petrogenesis of the eastern Pyrenean peridotites: an integrated study of their whole-rock geochemistry and Re-Os isotope composition. Geochim. Cosmochim. Acta 62, 2293–2310.

Chen, G., Xia, B., 2008. Platinum-group elemental geochemistry of mafic and ultramafic rocks from the Xigaze ophiolite, southern Tibet. J. Asian Earth Sci. 32 (5–6), 406–422.

Chu, Z.Y., Wu, F.Y., Walker, R.J., Rudnick, R.L., Pitcher, L., Puchtel, I.S., Yang, Y.H., Wilde, S.A., 2009. Temporal evolution of the lithospheric mantle beneath the eastern North China Craton. J. Petrol. 50, 1857–1898.

Cohen, A.S., Waters, F.G., 1996. Separation of osmium from geological materials by solvent extraction for analysis by thermal ionisation mass spectrometry. Anal. Chim. Acta 332, 269–275.

Cushman, B., Sinton, J., Ito, G., Dixon, J.E., 2004. Glass compositions, plume-ridge interaction, and hydrous melting along the Galápagos spreading center, 90.5°W to 98°W. Geochem. Geophys. Geosyst. 5. https://doi.org/10.1029/2004GC000709 Q08E17.

Dai, J.G., Wang, C.S., Hébert, R., Santosh, M., Li, Y.L., Xu, J.Y., 2011. Petrology and geochemistry of peridotites in the Zhongba ophiolite, Yarlung Zangbo Suture Zone: implications for the early cretaceous intra-oceanic subduction zone within the Neo-Tethys. Chem. Geol. 288 (3–4), 133–148.

Day, J.M., Walker, R.J., Warren, J.M., 2017. ^{186}Os–^{187}Os and highly siderophile element abundance systematics of the mantle revealed by abyssal peridotites and Os-rich alloys. Geochim. Cosmochim. Acta 200, 232–254.

Deng, J., Wang, Q., Li, G., Li, C., Wang, C., 2014. Tethys tectonic evolution and its bearing on the distribution of important mineral deposits in the Sanjiang region, SW China. Gondwana Res. 26, 419–437.

Dick, H.J., Bullen, T., 1984. Chromian spinel as a petrogenetic indicator in abyssal and alpine-type peridotites and spatially associated lavas. Contrib. Mineral. Petrol. 86, 54–76.

Dilek, Y., Furnes, H., 2011. Ophiolite genesis and global tectonics: geochemical and tectonic fingerprinting of ancient oceanic lithosphere. Geol. Soc. Am. Bull. 123, 387–411.

Dilek, Y., Furnes, H., 2014. Ophiolites and their origins. Elements 10 (2), 93–100.

Evans, B.W., Hattori, K., Baronnet, A., 2013. Serpentinite: what, why, where? Elements 9 (2), 99–106.

Faure, M., Lin, W., Chu, Y., Lepvrier, C., 2016. Triassic tectonics of the southern margin of the South China block. Compt. Rendus Geosci. 348, 5–14.

Fischer-Gödde, M., Becker, H., Wombacher, F., 2011. Rhodium, gold and other highly siderophile elements in orogenic peridotites and peridotite xenoliths. Chem. Geol. 280 (3), 365–383.

Gaetani, G.A., Grove, T.L., 1998. The influence of water on melting of mantle peridotite. Contrib. Mineral. Petrol. 131, 323–346.

Grove, T.L., Chatterjee, N., Parman, S.W., Médard, E., 2006. The influence of H_2O on mantle wedge melting. Earth Planet. Sci. Lett. 249 (1–2), 74–89.

Gruau, G., Bernard-Griffiths, J., Lécuyer, C., 1998. The origin of U-shaped rare earth patterns in ophiolite peridotites: assessing the role of secondary alteration and melt/rock reaction. Geochim. Cosmochim. Acta 62 (21—22), 3545–3560.

Hart, S.R., Zindler, A., 1986. In search of a bulk-earth composition. Chem. Geol. 57, 247–267.

Harvey, J., Gannoun, A., Burton, K.W., Rogers, N.W., Alard, O., Parkinson, I.J., 2006. Ancient melt extraction from the oceanic upper mantle revealed by Re–Os isotopes in abyssal peridotites from the Mid-Atlantic ridge. Earth Planet. Sci. Lett. 244 (3), 606–621.

Hellerbrand, E., Snow, J.E., Dick, H.J.B., Hofman, A.W., 2001. Coupled major and trace elements as indicators of the extent of melting in Mid-Ocean-Ridge peridotite. Nature 410 (6829), 677–681.

Hu, W.J., Zhong, H., Zhu, W.G., He, X.H., 2015. Elemental and Sr–Nd isotopic geochemistry of the basalts and microgabbros in the Shuanggou ophiolite, SW China: implication for the evolution of the Palaeotethys Ocean. Geol. Mag. 152 (2), 210–224.

Hu, W.J., Zhong, H., Zhu, W.G., Bai, Z.J., 2019. Rift- and subduction-related crustal sequences in the Jinshajiang ophiolitic mélange, SW China: Insights into the eastern Paleo-Tethys. Lithosphere 11 (6), 821–833.

Hu, W.J., Zhong, H., Chu, Z.Y., Zhu, W.G., Bai, Z.J., Zhang, C., 2020. Ancient refertilization process preserved in the plagioclase peridotites: an example from the Shuanggou ophiolite, southwest China. J. Geophys. Res. Solid Earth 125 (1). https://doi.org/10.1029/2019JB017552 e2019JB017552.

Hyndman, R.D., Peacock, S.M., 2003. Serpentinization of the forearc mantle. Earth Planet. Sci. Lett. 212 (3–4), 417–432.

Ishii, T., Robinson, P.T., Maekawa, H., Fiske, R., 1992. Petrological studies of peridotites from diapiric serpentinite seamounts in the Izu-Ogasawara-Mariana forearc, Leg 125. Proceedings of the Ocean Drilling Program, Scientific Results. 125, pp. 445–485.

Jian, P., Liu, D.Y., Sun, X.M., 2008. SHRIMP dating of the Permo-Carboniferous Jinshajiang ophiolite, southwestern China: Geochronological constraints for the evolution of Paleo-Tethys. J. Asian Earth Sci. 32, 371–384.

Jian, P., Liu, D.Y., Kroner, A., Zhang, Q., Wang, Y.Z., Sun, X.M., Zhang, W., 2009a. Devonian to Permian plate tectonic cycle of the Paleo-Tethys Orogen in Southwest China (I): Geochemistry of ophiolites, arc/back-arc assemblages and within-plate igneous rocks. Lithos 113, 748–766.

Jian, P., Liu, D.Y., Kroner, A., Zhang, Q., Wang, Y.Z., Sun, X.M., Zhang, W., 2009b. Devonian to Permian plate tectonic cycle of the Paleo-Tethys Orogen in Southwest China (II): Insights from zircon ages of ophiolites, arc/back-arc assemblages and within-plate igneous rocks and generation of the Emeishan CFB province. Lithos 113, 767–784.

Kelemen, P.B., 1990. Reaction between ultramafic rock and fractionating basaltic magma 1. Phase-relations, the origin of calc-alkaline magma series, and the formation of discordant dunite. J. Petrol. 31, 51–98.

Kelemen, P.B., Dick, H.J.B., Quick, J.E., 1992. Formation of harzburgite by pervasive melt/rock reaction in the upper mantle. Nature 358, 635–641.

Kelemen, P.B., Shimizu, N., Salters, V.J.M., 1995. Extraction of mid-ocean-ridge basalt from the upwelling mantle by focused flow of melt in dunite channels. Nature 375, 747–753.

Kelemen, P.B., Hirth, G., Shimizu, N., Spiegelman, M., Dick, H.J.B., 1997. A review of melt migration processes in the adiabatically upwelling mantle beneath oceanic spreading ridges. Philosophical Transactions of the Royal Society a-Mathematical Physical and Engineering Sciences 355, 283–318.

Kushiro, I., Syono, Y., Akimoto, S., 1968. Melting of a peridotite nodule at high pressures and high water pressures. J. Geophys. Res. 73 (18), 6023–6029.

Le Roux, P.J., Le Roex, A.P., Schilling, J.G., Shimizu, N., Perkins, W.W., Pearce, N.J.G., 2002. Mantle heterogeneity beneath the southern Mid-Atlantic Ridge: Trace element evidence for contamination of ambient asthenospheric mantle. Earth Planet. Sci. Lett. 203, 479–498.

Le Roux, V., Bodinier, J.L., Tommasi, A., Alard, O., Dautria, J.M., Vauchez, A., Riches, A.J.V., 2007. The Lherz spinel lherzolite: refertilized rather than pristine mantle. Earth Planet. Sci. Lett. 259, 599–612.

Leloup, P.H., Lacassin, R., Tapponnier, P., Schärer, U., Zhong, D., Liu, X., Zhang, L., Ji, S., Trinh, P.T., 1995. The Ailao Shan-Red River shear zone (Yunnan, China), Tertiary transform boundary of Indochina. Tectonophysics 251, 3–84.

Li, X., Jiang, X., Sun, Z., Shen, G., Du, D., 2002. The Collision Orogenic Processes of the Nujiang LancangjiangJinshajiang Area, SW China. Geological Publishing House, Beijing, p. 213 (in Chinese).

Li, W.C., Pan, G.T., Hou, Z.Q., Mo, X.X., Wang, L.Q., Ding, J., 2010. Metallogenic and Exploration Techniques of Multi-Island-Arc Basin-Collision Orogenic Belt in Southwest the "Three Rivers". Geological Publishing House, Beijing, p. 107 (in Chinese).

Liu, Z.R.R., Zhou, M.F., 2017. Meishucun phosphorite succession (SW China) records redox changes of the early Cambrian Ocean. Geol. Soc. Am. Bull. 129 (11—12), 1554–1567.

Liu, C.Z., Snow, J.E., Hellebrand, E., Brügmann, G., Von Der Handt, A., Büchl, A., Hofmann, A.W., 2008. Ancient, highly heterogeneous mantle beneath Gakkel ridge, Arctic Ocean. Nature 452 (7185), 311.

Liu, J.G., Rudnick, R.L., Walker, R.J., Gao, S., Wu, F.Y., Piccoli, P.M., 2010a. Processes controlling highly siderophile element fractionations in xenolithic peridotites and their influence on Os isotopes. Earth Planet. Sci. Lett. 297, 287–297.

Liu, J.G., Scott, J.M., Martin, C.E., Pearson, D.G., 2015. The longevity of Archean mantle residues in the convecting upper mantle and their role in young continent formation. Earth Planet. Sci. Lett. 424, 109–118.

Liu, T., Wu, F.Y., Liu, C.Z., Zhang, C., Ji, W.B., Xu, Y., 2019a. Reconsideration of Neo-Tethys evolution constrained from the nature of the Dazhuqu ophiolitic mantle, southern Tibet. Contrib. Mineral. Petrol. 174, 23. https://doi.org/10.1007/s00410-019-1557-7.

Liu, Z.R.R., Zhou, M.F., Williams-Jones, A.E., Wang, W., Gao, J.F., 2019b. Diagenetic mobilization of Ti and formation of brookite/anatase in early Cambrian black shales, South China. Chem. Geol. 506, 79–96.

Lorand, J.P., Luguet, A., Alard, O., 2008. Platinum-group elements: a new set of key tracers for the earth's interior. Elements 4, 247–252.

Lorand, J.P., Luguet, A., Alard, O., 2013. Platinum-group element systematics and petrogenetic processing of the continental upper mantle: a review. Lithos 164, 2–21.

McDonough, W.F., Sun, S.S., 1995. The composition of the Earth. Chem. Geol. 120, 223–253.

Meisel, T., Walker, R.J., Irving, A.J., Lorand, J.P., 2001. Osmium isotopic compositions of mantle xenoliths: a global perspective. Geochim. Cosmochim. Acta 65 (8), 1311–1323.

Metcalfe, I., 2006. Paleozoic and Mesozoic tectonic evolution and palaeogeography of East Asian crustal fragments: the Korean Peninsula in context. Gondwana Res. 9, 24–46.

Metcalfe, I., 2011. Palaeozoic–Mesozoic history of SE Asia. Geol. Soc. Lond., Spec. Publ. 355, 7–35.

Metcalfe, I., 2013. Gondwana dispersion and Asian accretion: Tectonic and palaeogeographic evolution of eastern Tethys. J. Asian Earth Sci. 66, 1–33.

Mével, C., 2003. Serpentinization of abyssal peridotites at mid-ocean ridges. Compt. Rendus Geosci. 335 (10—11), 825–852.

Miyashiro, A., 1973. The Troodos ophiolitic complex was probably formed in an island arc. Earth Planet. Sci. Lett. 19 (2), 218–224.

Mo, X.X., Shen, S.Y., Zhu, Q.W., Xu, T.R., Wei, Q.R., Tan, J., Zhang, S.Q., Cheng, H.L., 1998. Volcanics-Ophiolite and Mineralization of Middle-Southern Part in Sanjiang Area of Southwestern China. Geological Publishing House, Beijing, p. 128 (in Chinese).

Montanini, A., Tribuzio, R., Vernia, L., 2008. Petrogenesis of basalts and gabbros from an ancient continent–ocean transition (External Liguride ophiolites, Northern Italy). Lithos 101 (3–4), 453–479.

Mou, C., Wang, L., 2000. The evolution of the volcanosedimentary basin during the late Triassic in Deqen, Yunnan. J. Mineral. Petrol. 20, 23–28 (in Chinese with English abstract).

Mungall, J.E., Naldrett, A.J., 2008. Ore deposits of the platinum-group elements. Elements 4, 253–258.

Niu, Y.L., 2004. Bulk-rock major and trace element compositions of abyssal peridotites: Implications for mantle melting, melt extraction and post-melting processes beneath mid-ocean ridges. J. Petrol. 45, 2423–2458.

O'Driscoll, B., Day, J.M., Walker, R.J., Daly, J.S., McDonough, W.F., Piccoli, P.M., 2012. Chemical heterogeneity in the upper mantle recorded by peridotites and chromitites from the Shetland Ophiolite complex, Scotland. Earth Planet. Sci. Lett. 333, 226–237.
O'Reilly, S.Y., Zhang, M., Griffin, W.L., Begg, G., Hronsky, J., 2009. Ultradeep continental roots and their oceanic remnants: a solution to the geochemical "mantle reservoir" problem? Lithos 112, 1043–1054.
Pamić, J., Tomljenović, B., Balen, D., 2002. Geodynamic and petrogenetic evolution of Alpine ophiolites from the central and NW Dinarides: an overview. Lithos 65 (1–2), 113–142.
Parkinson, I.J., Pearce, J.A., 1998. Peridotites from the Izu–Bonin–Mariana forearc (ODP Leg 125): evidence for mantle melting and melt–mantle interaction in a supra-subduction zone setting. J. Petrol. 39, 1577–1618.
Parkinson, I.J., Hawkesworth, C.J., Cohen, A.S., 1998. Ancient mantle in a modern arc: Osmium isotopes in Izu-Bonin-Mariana forearc peridotites. Science 281, 2011–2013.
Paulick, H., Bach, W., Godard, M., De Hoog, J.C.M., Suhr, G., Harvey, J., 2006. Geochemistry of abyssal peridotites (Mid-Atlantic Ridge, 15°20′N, ODP Leg 209): Implications for fluid/rock interaction in slow spreading environments. Chem. Geol. 234 (3–4), 179–210.
Pearce, J.A., 2014. Immobile Element Fingerprinting of Ophiolites. Elements 10 (2), 101–108.
Pearce, J.A., Robinson, P.T., 2010. The Troodos ophiolitic complex probably formed in a subduction initiation, slab edge setting. Gondwana Res. 18 (1), 60–81.
Pearce, J.A., Barker, P.F., Edwards, S.J., Parkinson, I.J., Leat, P.T., 2000. Geochemistry and tectonic significance of peridotites from the South Sandwich arc–basin system, South Atlantic. Contrib. Mineral. Petrol. 139, 36–53.
Qi, L., Hu, J., Grégoire, D.C., 2000. Determination of trace elements in granites by inductively coupled plasma mass spectrometry. Talanta 51, 507–513.
Qi, L., Gao, J., Huang, X., Hu, J., Zhou, M.F., Zhong, H., 2011. An improved digestion technique for determination of platinum group elements in geological samples. J. Anal. At. Spectrom. 26, 1900–1904.
Rampone, E., Hofmann, A.W., 2012. A global overview of isotopic heterogeneities in the oceanic mantle. Lithos 148, 247–261.
Rudnick, R.L., Walker, R.J., 2009. Interpreting ages from Re-Os isotopes in peridotites. Lithos 112, 1083–1095.
Schaltegger, U., Desmurs, L., Manatschal, G., Müntener, O., Meier, M., Frank, M., Bernoulli, D., 2002. The transition from rifting to sea-floor spreading within a magma-poor rifted margin: field and isotopic constraints. Terra Nova 14 (3), 156–162.
Schmidt, M.W., Poli, S., 1998. Experimentally based water budgets for dehydrating slabs and consequences for arc magma generation. Earth Planet. Sci. Lett. 163 (1–4), 361–379.
Schulte, R.F., Schilling, M., Anma, R., Farquhar, J., Horan, M.F., Komiya, T., Piccoli, P.M., Pitcher, L., Walker, R.J., 2009. Chemical and chronologic complexity in the convecting upper mantle: evidence from the Taitao ophiolite, southern Chile. Geochim. Cosmochim. Acta 73 (19), 5793–5819.
Scott, J.M., Liu, J.G., Pearson, D.G., Harris, G.A., Czertowicz, T.A., Woodland, S.J., Riches, A.J.V., Luth, R.W., 2019. Continent stabilisation by lateral accretion of subduction zoneprocessed depleted mantle residues; insights from Zealandia. Earth Planet. Sci. Lett. 507, 175–186.
Snow, J.E., Reisberg, L., 1995. Os isotopic systematics of the MORB mantle: results from altered abyssal peridotites. Earth Planet. Sci. Lett. 133 (3–4), 411–421.
Sun, X., Jian, P., 2004. The Wilson cycle of the Jinshajiang Paleo-Tethys Ocean, in western Yunnan and Sichuan Provinces. Geol. Rev. (Dizhi Lunping) 50, 343–350 (in Chinese).
Sun, S.S., McDonough, W.F., 1989. Chemical and isotopic systematics of oceanic basalts: implications formantle composition and processes. Geol. Soc. Lond., Spec. Publ. 42, 313–345.
Tan, F., 2002. The sedimentary characteristics of Simao Triassic rear arc foreland basin, Yunnan Province. Acta Sedimentol. Sin. 20, 560–567 (in Chinese with English abstract).
Wang, P., 1985. Petrochemistry of the ophiolite-associated lavas in Deqin, Yunnan. Contribution of the Geology of the Qinhai-Xizang (Tibet) Plateau 9, 207–219 (in Chinese with English abstract).
Wang, X.F., Metcalfe, I., Jian, P., He, L.Q., Wang, C.S., 2000a. The Jinshajiang-Ailaoshan Suture Zone, China: tectonostratigraphy, age and evolution. J. Asian Earth Sci. 18, 675–690.
Wang, Y.Z., Li, X.L., Duan, L.I., Huang, Z.X., Chui, C., 2000b. Geotectonics and Metallogeneny in South Nujiang-Lanchang-Jinsha Rivers Area. Geologial Publishing House, Beijing (in Chinese).
Wang, Y.J., Fan, W.M., Zhang, Y.H., Peng, T.P., Chen, X.Y., Xu, Y.G., 2006. Kinematics and Ar^{40}/Ar^{39} geochronology of the Gaoligong and Chongshan shear systems, western Yunnan, China: Implications for early Oligocene tectonic extrusion of SE Asia. Tectonophysics 418, 235–254.
Wang, D.B., Wang, L.Q., Yin, F.G., Sun, Z.M., Wang, B.D., Zhang, W.P., 2012. Timing and nature of the Jinshajiang Paleo-Tethys: Constraints from zircon U-Pb age and Hf isotope of the Dongzhulin layered gabbro from Jinshajiang ophiolite belt, northwestern Yunnan. Acta Petrol. Sin. 28 (5), 1542–1550 (in Chinese with English abstract).
Wang, Y.J., Qian, X., Cawood, P.A., Liu, H.C., Feng, Q.L., Zhao, G.C., Zhang, Y.H., He, H.Y., Zhang, P.Z., 2018. Closure of the East Paleotethyan Ocean and amalgamation of the Eastern Cimmerian and Southeast Asia continental fragment. Earth Sci. Rev. 186, 195–230.
Warren, J.M., 2016. Global variations in abyssal peridotite compositions. Lithos 248, 193–219.
Wei, G.Y., Feng, G.R., Luo, Z.W., Wu, S.Z., Tao, Y.Y., 1984. Stratigraphic sequences of the Lancang and Chongshan groups in western Yunnan and their volcanism and metamorphism. J. Chengdu Coll. Geol. 2, 12–20 (in Chinese with English abstract).
Workman, R.K., Hart, S.R., 2005. Major and trace element composition of the depleted MORB mantle (DMM). Earth Planet. Sci. Lett. 231, 53–72.
Wu, S.Z., Tao, Y.Y., Feng, G.R., Wei, G.Y., Luo, Z.W., 1984. Metavolcanics in the Langcang Goup and the Chongshan Group. Yunnan Geol. 3, 113–123 (in Chinese).
Xiao, L., He, Q., Pirajno, F., Ni, P., Du, J., Wei, Q., 2008. Possible correlation between a mantle plume and the evolution of Paleo-Tethys Jinshajiang Ocean: evidence from a volcanic rifted margin in the Xiaru-Tuoding area, Yunnan, SW China. Lithos 100, 112–126.
Xiong, Q., Griffin, W.L., Zheng, J.P., O'Reilly, S.Y., Pearson, N.J., Xu, B., Belousova, E.A., 2016. Southward trench migration at ~130–120 Ma caused accretion of the Neo-Tethyan forearc lithosphere in Tibetan ophiolites. Earth Planet. Sci. Lett. 438, 57–65.
Xiong, Q., Griffin, W.L., Zheng, J.P., Pearson, N.J., O'Reilly, S.Y., 2017. Two-layered oceanic lithospheric mantle in a Tibetan ophiolite produced by episodic subduction of Tethyan slabs. Geochem. Geophys. Geosyst. 18, 1189–1213.
Xiong, Q., Xu, Y., González-Jiménez, J.M., Liu, J.G., Alard, O., Zheng, J.P., Griffin, W.L., O'Reilly, S.Y., 2020. Sulfide in dunite channels reflects long-distance reactive migration of mid-ocean-ridge melts from mantle source to crust: a Re-Os isotopic perspective. Earth Planet. Sci. Lett. 531, 115969. https://doi.org/10.1016/j.epsl.2019.115969.
Xu, Y., Liu, J.G., Xiong, Q., Su, B.X., Scott, J.M., Xu, B., Zhu, D.C., Pearson, D.G., 2020. The complex life cycle of oceanic lithosphere: a study of Yarlung-Zangbo ophiolitic peridotites, Tibet. Geochim. Cosmochim. Acta 277, 175–191.
Yang, K.H., Mo, X.X., Zhu, Q.W., 1994. Tectono-volcanic belts and late Paleozoic–early Mesozoic evolution of southwestern Yunnan, China. J. SE Asian Earth Sci. 10, 245–262.
Zhang, P.F., Uysal, I., Zhou, M.F., Su, B.X., Avc, E., 2016. Subduction initiation for the formation of high-Cr chromitites in the Kop ophiolite, NE Turkey. Lithos 260, 345–355.
Zhang, P.F., Zhou, M.F., Robinson, P.T., Pearce, J.A., Malpas, J., Liu, Q.Y., Xia, X.P., 2019. Evolution of nascent mantle wedges during subduction initiation: Li-O isotopic evidence from the Luobusa ophiolite, Tibet. Geochim. Cosmochim. Acta 245, 35–58.
Zhang, Q., Zhou, D., Zhao, D., 1996. Wilson cycle of the Paleo-Tethyan orogenic belt in western Yunnan: record of magmatism and discussion on mantle processes. Acta Petrol. Sin. 12, 17–28 (in Chinese with English abstract).
Zhong, D.L., 1998. Paleo-Tethyan Orogenic Belt in Western Yunnan and Sichuan. Science Press, Beijing (in Chinese).
Zhou, M.F., Robinson, P.T., Malpas, J., Edwards, S.J., Qi, L., 2005. REE and PGE geochemical constraints on the formation of dunites in the Luobusa Ophiolite, Southern Tibet. J. Petrol. 46 (3), 615–639.
Zi, J.W., Cawood, P.A., Fan, W.M., Tohver, E., Wang, Y.J., McCuaig, T.C., 2012a. Generation of early Indosinian enriched mantle-derived granitoid pluton in the Sanjiang orogen (SW China) in response to closure of the PaleoTethys. Lithos 140, 166–182.
Zi, J.W., Cawood, P.A., Fan, W.M., Wang, Y.J., Tohver, E., 2012b. Contrasting rift and subduction-related plagiogranites in the Jinshajiang ophiolitic mélange, Southwest China, and implications for the Paleo-Tethys. Tectonics 31 TC2012.
Zi, J.W., Cawood, P.A., Fan, W.M., Wang, Y.J., Tohver, E., McCuaig, T.C., Peng, T.P., 2012c. Triassic collision in the Paleo-Tethys Ocean constrained by volcanic activity in SW China. Lithos 144, 145–160.
Zi, J.W., Cawood, P.A., Fan, W.M., Tohver, E., Wang, Y.J., McCuaig, T.C., Peng, T.P., 2013. Late Permian–Triassic magmatic evolution in the Jinshajiang orogenic belt, SW China, and implications for orogenic processes following closure of the Paleo-Tethys. Am. J. Sci. 313, 81–112.